Growth and collapse of a vapor bubble in a narrow tube

E. Ory, H. Yuan, A. Prosperetti, S. Popinet, S. Zaleski

Growth and Collapse of a Vapor Bubble in a Narrow Tube

E. Ory, H. Yuan and A. Prosperetti*

Department of Mechanical Engineering

The Johns Hopkins University

Baltimore MD 21218 U.S.A.

S. Popinet and S. Zaleski

Laboratoire de Modélisation en Mécanique UMR–CNRS 7607

Université Pierre et Marie Curie

4 place Jussieu, 75252 Paris Cedex 05, France

(January 9, 2000)

Abstract

The fluid mechanical aspects of the axisymmetric growth and collapse of a bubble in a narrow tube filled with a viscous liquid are studied numerically. The tube is open at both ends and connects two liquid reservoirs at constant pressure. The bubble is initially a small sphere and growth is triggered by a large internal pressure applied for a short time. After this initial phase, the motion proceeds by inertia. This model simulates the effect of an intense, localized, brief heating of the liquid which leads to the nucleation and growth of a bubble. The dimensionless parameters governing the problem are discussed and their effects illustrated with several examples. It is also shown that, when

*Also: Department of Applied Physics, Twente Institute of Mechanics, and Burgerscentrum, University of Twente, AE 7500 Enschede, The Netherlands.

the bubble is not located at the midpoint of the tube, a net flow develops capable of pumping fluid from one reservoir to the other. The motivation for this work is offered by the possibility to use vapor bubbles as actuators in fluid–handling microdevices.

PACS Nos.: 47.55.Dz, 47.60.+i, 47.11.+j

I. INTRODUCTION

In an ink–jet printer drops are produced and ejected due to the rapid growth of bubbles in a narrow flow passage just upstream of the nozzle exit (see e.g. Ref. [2,1,5]). This is but one example of the possible application of vapor bubbles in small devices, where they offer the interesting potential of mechanical actuation, pumping, and other flow effects without mechanical moving parts. In these situations bubbles are produced by small heaters in the tube wall to which a brief current pulse is applied. A very small mass of liquid reaches a temperature comparable with the critical temperature, and a vapor bubble nucleates and rapidly grows. In a recent paper we have studied the thermal and attendant phase–change processes that take place in such a situation [18]. We found that, due to the work of expansion and vapor condensation on the cold liquid surface, the initial high vapor pressure in the bubble is very quickly dissipated. The rest of the bubble evolution essentially proceeds by inertia. In that study the fluid mechanical aspects of the problem were treated by means of a simplified model based on potential flow and an approximate treatment of viscous effects. The purpose of this article is to simulate the actual flow behavior by solving numerically the full Navier–Stokes equations. We shall however simplify the thermal problem by assuming that the bubble internal pressure at time 0 is briefly raised to a level Δp above the saturation level $p_0 \simeq 0$ corresponding to the undisturbed liquid temperature. This high internal overpressure is maintained for a time τ, after which it falls to zero again. In another recent paper [19] we have compared the results of this simple model with the one of Ref. [18] finding a very good agreement.

The advancing of a gas bubble in a tube is a classic problem treated by many others since the early work of Bretherton [3]; Ref. [10] gives a good review and some more recent work can be found in Refs. [6,7]. The situation considered in this paper is however different as, first, the bubble undergoes a significant volume change and, second, the flow is highly transient as opposed to the steady or quasi–steady situations considered before. In addition, inertial effects are significant and therefore we deal with the full Navier–Stokes equations,

rather than the Stokes equations as many of the previous authors. The situation considered in the study of boiling in porous media (see e.g. Ref. [12,15,11,17]) is also quite different from the present one as, in that case, heat is added to the system continuously from the entire pore wall, rather than locally and impulsively as here. Among the earlier work on the specific problem studied here, the closest one is that of Asai et al. [2] who, however, developed a quasi–one–dimensional model and were chiefly concerned with drop formation in the ink–jet system rather than with specific fluid mechanical phenomena.

An interesting and unexpected result that we find is that a single bubble cyclically growing and collapsing away from the midpoint of the channel is capable of inducing a mean uni–directional flow capable of pumping liquid from one reservoir to the other.

II. PRELIMINARY CONSIDERATIONS

We consider a tube of length L and inner diameter D connecting two liquid reservoirs at the same pressure P_∞ (Fig. 1). We simplify the problem by assuming axial symmetry and, at the initial instant, place a small spherical bubble of diameter D_i on the axis at the center of the tube. The pressure in the bubble is maintained at the level $p_0 + \Delta p$ for $0 \leq t < \tau$, after which it falls to p_0 for the remainder of the growth and collapse cycle; p_0 is the saturated vapor pressure at the undisturbed liquid temperature.

On the basis of a simple conceptual model according to which, in its growth, the bubble pushes in opposite directions two equal liquid columns of length $\frac{1}{2}L$ with an acceleration $(\Delta p + p_0 - P_\infty)/\frac{1}{2}L\rho$, we find that a characteristic velocity scale for the problem is

$$V = \frac{\Delta p + p_0 - P_\infty}{\frac{1}{2}L\rho}\,\tau\,, \tag{1}$$

where τ is the duration of the high–pressure phase. In terms of this characteristic velocity we define Reynolds, Strouhal, and Weber numbers in the usual way by

$$Re = \frac{\rho V D}{\mu}\,, \qquad St = \frac{D}{V\tau}\,, \qquad We = \frac{D\rho V^2}{\sigma}\,. \tag{2}$$

Here ρ, μ, and σ are the density, viscosity, and surface tension coefficients of the liquid. It should be noted that the velocity V defined by (1) is of the order of the peak velocity during the process and, therefore, the value of the Reynolds number defined here tends to underestimate the magnitude of viscous effects. In the literature the capillary number $Ca = We/Re$ is also frequently encountered, but its significance here is somewhat obscured by the highly transient nature of the phenomenon investigated.

Other parameters characterizing the problem are the ratio of the applied overpressure to the pressure difference $P_\infty - p_0$ that tends to collapse the bubble:

$$\mathcal{P} = \frac{\Delta p}{P_\infty - p_0}, \tag{3}$$

the aspect ratio of the channel:

$$\mathcal{A} = \frac{L}{D}, \tag{4}$$

and the ratio of the initial bubble diameter D_i to the channel diameter:

$$\mathcal{D} = \frac{D_i}{D}. \tag{5}$$

Other quantities of interest can be expressed in terms of the previous parameters. For example, the ratio of the viscous diffusion time to the capillary wave period is

$$\mathcal{T}_d = \frac{D^2}{\nu}\sqrt{\frac{\sigma}{\rho D^3}} = \frac{Re}{\sqrt{We}}. \tag{6}$$

This quantity (which equals the square root of the Laplace number or the inverse of the Ohnesorge number), may also be interpreted as the order of the number of periods necessary for viscosity to damp out the longest capillary waves that the system can support.

We shall compare the results with those of a simplified model developed in earlier work in which the bubble is approximated as a cylinder occupying the entire cross section of the tube, with some provisions made for surface tension and viscous effects [18]. A full description and a complete numerical solution are presented in [19]. If the model is further simplified neglecting surface tension effects, interfacial curvature, and viscosity, it lends itself

to an approximate analysis and a consideration of the results found in this way is useful to interpret the numerical ones presented below. For simplicity we only consider the simplified solution valid provided the bubble surfaces remain sufficiently far from the tube ends. With this assumption it can be shown that the maximum horizontal extension X_m of the bubble is:

$$X_m \simeq \frac{\Delta p + p_0 - P_\infty}{P_\infty - p_0} \frac{\Delta p\, \tau^2}{\frac{1}{2}\rho\, L}\,. \tag{7}$$

In the context of this simple model the bubble is a cylinder and therefore its maximum volume is $\mathcal{V}_{max} = \frac{1}{4}\pi D^2 X_m$ or, in dimensionless form,

$$\frac{\mathcal{V}_{max}}{\frac{1}{4}\pi D^2 L} = \frac{\mathcal{P}}{\mathcal{A}\, St}\,. \tag{8}$$

On the basis of the same simple model one finds that the processes of growth and collapse are nearly the mirror image of each other and that the bubble lifetime t_B is given by

$$\frac{t_B}{\tau} \simeq 2\,\mathcal{P}\,, \tag{9}$$

or

$$\frac{V t_B}{L} = \frac{2\,\mathcal{P}}{\mathcal{A}\, St}\,. \tag{10}$$

With the aid of these relations we have the following expression for the ratio of the viscous diffusion length to the tube diameter:

$$\mathcal{T}_v = \frac{\sqrt{t_B \nu}}{D} = \sqrt{\frac{2\mathcal{P}}{St\, Re}}\,. \tag{11}$$

This parameter can also be interpreted as the ratio of the viscous diffusion time to the bubble lifetime. Another significant parameter is the ratio of the period of capillary waves with wavelength of the order of D to the bubble lifetime:

$$\mathcal{T}_\sigma = \sqrt{\frac{\rho D^3}{\sigma\, t_B^2}} = \frac{St}{2\mathcal{P}}\sqrt{We}\,. \tag{12}$$

This parameter gives an idea of the number of capillary wave periods during the bubble life.

III. THE MODEL

We solve numerically, by a method briefly described later, the standard full, incompressible, viscous Navier–Stokes equations in the interior of the tube. Since only a minute amount of liquid is heated, and only for a brief fraction of the duration of the process, we treat the fluid properties constant. The usual no–slip condition is applied at the walls. At the bubble surface the normal stress is taken to equal the internal bubble pressure corrected for surface tension effects while the tangential stress vanishes. The boundary conditions at the tube ends are less straightforward and require some discussion.

The simplest option is to impose that the pressure at the tube ends is the undisturbed reservoir pressure P_∞. This choice can be justified during the growth phase of the bubble as, due to flow separation, the fluid issues from the tube ends similarly to a jet. Approximating the flow as parallel, and neglecting viscous effects in the flow induced by the jet in its surroundings, we then find that the pressure at the tube outlets is indeed approximately equal to P_∞. The accuracy of this prescription during the collapse phase, however, is harder to justify as the liquid now enters the tube ends essentially omnidirectionally in a fashion reminiscent of a sink flow. If we approximate the flow as potential, an application of the Bernoulli integral shows that the pressure at the tube's ends (index e) is given by

$$\frac{\partial \phi_e}{\partial t} + \frac{1}{2}\rho u_e^2 + P_e \;=\; P_\infty \,, \tag{13}$$

where ϕ_e is the velocity potential and u_e the local velocity, assumed uniform over the cross section. In the context of potential flow, it can be proven that the velocity potential ϕ_e satisfies [9,8]

$$\phi_e \pm \frac{1}{2} D u_e \;=\; 0 \,, \tag{14}$$

where the upper sign is for the left end and the lower sign for the right end of the tube. With this relation we then find

$$P_e \;=\; P_\infty - \frac{1}{2}\rho u_e^2 - \frac{1}{2} D \rho \frac{\partial u_e}{\partial t} \,. \tag{15}$$

The last term can be shown to be negligible on the basis of the following argument. Integrate the momentum equation along the axis of the tube from the bubble surface to the tube end assuming a uniform velocity. This procedure gives

$$\ell(t)\,\frac{du_e}{dt} \;=\; \frac{P_e - P_b}{\rho}\,, \tag{16}$$

where ℓ is the length of the liquid column between the free surface and the tube end; the pressure in the liquid at the bubble surface, P_b, differs from the bubble internal pressure p_0 because of surface tension. Upon using this result to eliminate the liquid acceleration in (15) we find

$$P_e - P_\infty \;=\; -\frac{1}{2}\rho u_e^2 - \frac{1}{2}\frac{D}{\ell(t)}\,(P_e - P_b)\,. \tag{17}$$

In this paper we only consider situations such that $D \ll \ell$, and we therefore feel justified in dropping the last term. In principle, at the end of the collapse, if opposite sides of the bubble were to collide, P_b would suddenly become very large and this approximation could be inaccurate. We do not include this final stage of the collapse in the present simulations.

In summary, then, we set $P_e = P_\infty$ during bubble growth while, during collapse, we impose

$$P_e \;=\; P_\infty - \frac{1}{2}\rho u_e^2\,. \tag{18}$$

The switching between the two conditions is done at the moment of maximum bubble expansion when the velocity is essentially zero, which maintains a desirable degree of continuity. To estimate the relative importance of the second term in (18) it is useful to rewrite this equation in dimensionless form:

$$\frac{P_e}{P_\infty - p_0} \;=\; \frac{P_\infty}{P_\infty - p_0} - \frac{1}{2}\frac{\rho u_e^2}{P_\infty - p_0}\,. \tag{19}$$

Since $p_0 \ll P_\infty$ the first term in the right-hand side is very close to 1. The second term can be written as

$$\frac{1}{2}\frac{\rho u_e^2}{P_\infty - p_0} \;=\; \frac{1}{2}\frac{u_e^2(\mathcal{P}-1)}{\mathcal{A}StV^2}\,. \tag{20}$$

Since V is of the order of the maximum velocity and, for the cases considered here, the combination of dimensionless parameters appearing in this equation is not large, one would only expect a small contribution from this end correction, which is confirmed by the numerical results presented later in connection with Fig. 4.

All the results presented here are computed using a free–surface version of the code described in [20,16,14]. The full incompressible axisymmetric Navier–Stokes equations are solved by a projection method. The interface is discretized using a set of marker points linked by cubic splines. This description supplies the accurate knowledge of the position and curvature of the interface necessary to include the surface tension contribution. The marker points are advected by a simple bilinear interpolation scheme and are redistributed at every time step to insure a uniform distribution as the bubble deforms. Axial symmetry is enforced in the calculation. In the radial direction the integration domain extends between the axis and the wall of the tube, while in the axial direction it includes the entire tube length.

The interface velocity is calculated by extrapolation from the liquid region, which requires that a sufficient number of grid points exist between the bubble surface and the tube wall. To avoid an excessive grid refinement as this liquid layer gets thinner, we arbitrarily set the outward radial velocity of the interface to zero when it has advanced as far as a few grid points from the tube wall. By varying the number of grid points between 1 and 3, and by using different grids, we have verified that this procedure leads only to minute differences that are undetectable within the thickness of the lines used in the graphs. When the bubble is as close as this to the tube wall, the radial velocity of the interface is very small anyway. We have also conducted the standard grid refinement tests to verify the grid independence of the solutions that will be presented in the next section. Typically we used square cells with 32 grid points in the radial direction.

IV. RESULTS

Figure 2 shows the bubble shape at different instants of time during growth (upper panel) and collapse. In this as well as in all the examples that follow the bubble originates at the midpoint of the tube and therefore we only show the right half of the bubble. Note that the tube extends well beyond the right boundary of the figures all the way to $z/D = 16$. The dimensionless parameters have the following values: $Re = 306.25$, $St = 12.76$, $We = 21.44$, $\mathcal{P} = 50$, $\mathcal{A} = 32$, $\mathcal{D} = 0.1$ (see Table). Here and in the following figures (except the last two) the duration of the internal overpressure is $V\tau/L = 2.45\times10^{-3}$.

It may also be useful to have in mind a concrete physical realization of this system in terms of dimensional quantities. With the physical properties of water at 20 °C, the previous parameters would correspond e.g. to a 2 mm–long tube, with a diameter of 62.5 μm. The reservoir pressure is $P_\infty = 1$ atm, the overpressure Δp is 50 bars, and the overpressure duration is $\tau = 1$ μs; the characteristic velocity V is 4.9 m/s and the initial bubble diameter 6.25 μm.

As mentioned before, in the practical applications we envisage the initial temperature of the bubble surface would be of the order of 80% the critical temperature (see e.g. [1]). The corresponding saturation pressure would be much higher than the value of 50 bars used here. However, in that case, the bubble would start from a small nucleus and a large part of the initial overpressure would be expended in balancing surface tension and in expanding the nucleus. Since here we start already from a macroscopic bubble, and we keep the pressure overpressure constant until it falls to zero, rather than allowing it to gradually decay, the value that we use is realistic. This point was examined in Ref. [19] where it was shown that, assuming the product $\tau\Delta p$ equal to the time integral of the bubble internal overpressure resulted, in a good comparison with the results of a thermally more sophisticated model in which the initial bubble temperature was higher, but the cooling of the vapor was accounted for [18].

In Fig. 2 successive profiles are separated by $V\Delta t/L = 3.92\times10^{-3}$ dimensionless units

(corresponding, for the dimensional values given before, to 1.6 μs); hence the internal pressure has already fallen to p_0 before the second profile shown.

The bubble remains approximately spherical until it grows to occupy about 2/3 of the cross section. At that point preferential growth in the axial direction begins, with a relatively high curvature that gradually becomes more blunt as the flow slows down. The curvature of the end surfaces of the bubble during collapse remains relatively small and the motion is very nearly one–dimensional until the very end. The rapid reversal from an oblate to a prolate shape between the next to the last and the last contours shown is reminiscent of a similar phenomenon encountered in the collapse of a free, initially oblate bubble [4]. The phenomenon is caused by the fact that, when inertia dominates, the liquid velocity tends to be inversely correlated with the local radius of curvature of the interface.

The maximum dimensionless volume of the bubble predicted by (8) is in this case 0.122, to be compared with a calculated dimensionless volume of 0.076. In addition to the approximations inherent in (8), this difference is due to the fact that the precise bubble shape is rounded at the ends, which further decreases the volume with respect to the cylindrical shape assumed in (8). The bubble dimensionless lifetime estimated from (10) is 0.245, while the computed one is 0.187. The difference between the two is enhanced by the fact that the bigger bubble predicted by the simple model takes longer to collapse and has, therefore, a longer lifetime. The parameter $\mathcal{T}_v$ defined in (11) has the value 0.16, implying that viscous effects are only significant over a small fraction of the channel diameter. The thickness of the residual film near the wall is limited by the numerical considerations described in the previous section and therefore is not quantitatively significant here.

The capillary number evaluated from the formal relation $Ca = We/Re$ has the value 0.07. However, by using directly the definition $Ca = \mu V/\sigma$ with the computed time–dependent velocity, one finds values ranging approximately between 0.19 and 0, with most of the time $Ca < 0.03$–0.04. Thus surface tension is considerably less important than viscosity although, due to the transient nature of the flow, the results applicable to the steady case (see e.g. Ref. [6,7]) are not directly relevant here. The parameter $\mathcal{T}_\sigma$ defined in (12) equals 0.59, so

that the longest capillary waves have a period comparable with the bubble characteristic time, which explains the relative bluntness of the bubble ends. The parameter $\mathcal{T}_d$ of (6) is about 66, implying that capillary waves are only very lightly damped by viscosity.

A sixfold decrease in the Reynolds number from 306.25 to 51.04 (Fig. 3) produces a bubble about 20% shorter with a dimensionless lifetime of 0.159. Neither effect is contained in (7) and (9) which are evidently inapplicable to this relatively high–viscosity case. In qualitative agreement with the increased value of $\mathcal{T}_v$, the liquid film now is not limited by the numerics and is thicker than before, but the other general features of the process are not significantly affected. The increased damping of capillary waves ($\mathcal{T}_d$ is now about 11) permits a greater curvature of the bubble end surfaces. With a larger Reynolds number, one finds that the bubble maximum volume increases but little else changes with respect to the case of Fig. 2. The bubble volume vs. time is shown in Fig. 4 for different values of the Reynolds number. Here, as well as in Figs. 5, 10, and 13, time is made dimentionless according to

$$T^* = \frac{Vt}{L} = \frac{1}{\mathcal{A}\,St}\,\frac{t}{\tau}\,. \tag{21}$$

The dashed line shows the effect of modifying the boundary condition at the tube ends discussed in section III by simply imposing $P = P_\infty$ during both growth and collapse. The effect on the bubble dynamics is evidently rather small. The maximum volume and the bubble lifetime are shown vs. the Reynolds number in Fig. 5.

The bubble shape is markedly affected by an increase of the Weber number. Figure 6 is for an increase to $We = 120$. In the first place the bubble grows longer as the pressure drop across the interface necessary to balance the effect of surface tension is less. Secondly, the liquid film clearly has a non–uniform thickness as the reduced surface tension decreases the pressure gradient in the liquid due to curvature. Finally, the larger value of $\mathcal{T}_\sigma$ allows for the presence of capillary waves that are particularly evident during the collapse phase. If the Weber number is reduced to 10.72 (Fig. 7) the picture is similar to that of Fig. 2 for $We = 21.44$ except that, due to the capillary pressure drop, the bubble does not grow quite

as long.

All other things being equal, an increase in the Strouhal number means a shorter duration of the overpressure phase. The bubble grows therefore less, as implied by (8) and as shown in Fig. 8 for $St = 76.53$. The simple expression (8) predicts for this case a bubble dimensionless volume of 0.02, against the exact value of 0.017. For this case $\mathcal{T}_\sigma = 3.54$, and therefore capillary waves are prominent on the bubble surface. If St is reduced to 2.39 (Fig. 9) the bubble grows so large that the hypothesis under which the result (8) is derived is violated so that the predicted dimensionless volume, 0.65, is quite different from the actual computed value of 0.22. Figure 10 shows the bubble volume vs. time for several values of St. According to the relation (10), the dimensionless bubble lifetime should be inversely correlated with St, which is qualitatively verified. Quantitatively, (10) is only approximately correct for the larger Strouhal numbers due to the neglect of end effects.

Figures 11 and 12 illustrate the effect of increasing and decreasing the pressure parameter $\mathcal{P}$ whose influence on the volume vs. time is shown in Fig. 13. The proportionality of the bubble lifetime to $\mathcal{P}$ predicted by (9) is well verified provided the bubble does not grow too long.

Finally, the influence of the aspect ratio is illustrated in Figs. 14 ($\mathcal{A} = 8$) and 15 ($\mathcal{A} = 64$). When plotted versus z/D there is remarkably little difference between the two results in spite of the large variation in the aspect ratio. This finding is in approximate agreement with the result (7) that would predict $X_{max}/D \simeq \mathcal{P}/St$ independent of $\mathcal{A}$. The difference is however in the expected direction when the maximum volume is normalized as in (8): the bubble grows to occupy about 22% of the channel volume for $\mathcal{A} = 8$, but only about 4% for $\mathcal{A} = 64$. The bubble lifetime increases by about 30% going from $\mathcal{A} = 8$ to $\mathcal{A} = 64$.

The effect of the bubble initial diameter is small. It is found that increasing D_i/D from 0.1 to 0.8 only leads to a 20% increase in the maximum volume and a 10% increase in the bubble lifetime.

V. SINGLE–BUBBLE PUMPING

A very interesting phenomenon is encountered when the bubble grows and collapses away from the tube midpoint. An example is shown in Fig. 16 where the initial bubble nucleus is positioned 3/8 of the tube length away from the left end of the tube. Here all the dimensional parameters have the same values as in Fig. 2 except that $\tau = 2$ μs. As in the previous cases, the area shown in the figure is a small fraction of the computational domain that extends for $0 \leq z \leq 2000$ μm.

It is evident from the figure that the axial position where the collapse is completed – 859 μm from the tube left end – is different from that of the original bubble nucleus – 750 μm away from the tube left end. Thus, the bubble moves 109 μm (i.e., 1.74 tube diameters) away from the closest end of the tube. Since the bubble essentially occludes the tube during most of its life, this result suggests that the growth and collapse cycle is capable of imparting a net displacement to the liquid. This fact is confirmed by Fig. 17 which shows the liquid velocities on the tube axis at the two ends of the tube vs. time for this case. It is seen here that at the end of the collapse there is a residual positive net velocity, i.e. directed toward the end of the tube farther from the bubble.

Thus, by generating successive bubbles in a periodic fashion, one would be able to pump the liquid from one reservoir to the other one along the tube. Further considerations on this interesting and potentially useful effect can be found in Ref. [19].

Figure 16 presents also other elements of interest. In the first place, it is clear that the direction of motion does not reverse at the same time at the two ends of the bubble. Due to the greater inertia of the liquid column on the right, outward motion in this direction continues somewhat longer than that on the left. Secondly, there is a marked difference in shape between the two ends of the bubbles during growth and, especially, during collapse. Due to the different inertia of the liquid on the two sides of the bubble, the velocity with which the two interfaces displace is also different. The velocity of the left interface is relatively large, and the shape here has several features reminiscent of those encountered in

Fig. 6 where the large value of the Weber number, $We = 114.33$, also caused a prevailing of inertia over surface tension. The motion of the right bubble interface is instead relatively slow due to the large inertia of the longer right liquid column. Here, particularly at the beginning of the collapse, one encounters a tendency for the bubble surface to detach from the tube wall which is reminiscent of other slow collapse cases found before, e.g. in Fig. 8 for $St = 76.53$ or Fig. 12 for $\mathcal{P} = 12.5$.

VI. CONCLUSIONS

We have studied the fluid dynamics of the growth and collapse of a bubble in a small tube under the action of a short–lived internal overpressure. In a practical application, one would be interested in using the bubble growth to achieve mechanical actuation, possibly with a high repetition rate. The growth would be triggered by powering an electric heater for a short time to bring the temperature of a small liquid volume in the vicinity of the critical temperature.

In this note we have avoided the complexity of phase change and heat diffusion by applying a constant internal overpressure for a short time of the order of 1% of the total bubble lifetime. In spite of this brief duration, the expansion is mechanically very energetic without requiring a large amount of thermal energy. It should therefore be relatively easy to avoid a progressive increase of the system's temperature by dissipating heat by conduction through the tube walls, which is an essential requirement for achieving a fast repetition rate.

As shown in Ref. [18], in an actual application the cooling of the bubble occurs on a scale of microseconds because of the work of expansion and the conduction of heat into the surrounding cold liquid. After this time the temperature of the bubble remains essentially constant at the ambient value, the vapor pressure becomes negligible, and the entire dynamics are governed by inertia. This behavior is a consequence of the fact that, for a liquid such as water, the vapor density at normal temperature is so low that the latent heat required to maintain the bubble filled with saturated vapor can be supplied without altering appreciably

the temperature of the liquid at the liquid-vapor interface. The phenomenon is analogous in normal flow cavitation and the reader may consult e.g. Ref. [13] for more details and a quantitative argument.

Finally, a very interesting and somewhat surprising finding of this paper has been the pumping action described at the end of the previous section. This effect – which we have in the meantime demonstrated experimentally – could have useful practical applications and will be pursued in future work.

ACKNOWLEDGMENT

The portion of this work carried out at the Johns Hopkins University was supported by AFOSR under grant F49620–96–1–0386.

REFERENCES

[1] Asai, A., 1991, Bubble dynamics in boiling under high heat flux pulse heating, *J. Heat Transfer*, **113**, 973–979.

[2] Asai, A., Hara, T., & Endo, I., 1987, One–dimensional model of bubble growth and liquid flow in bubble jet printers, *Jap. J. Appl. Phys.*, **26**, 1794–1801.

[3] Bretherton, F.P., 1961, The motion of long bubbles in tubes, *J. Fluid Mech.*, **10**, 166–188.

[4] Chapman, R.B. & Plesset, M.S., 1972, Nonlinear effects in the collapse of a nearly spherical cavity in a liquid, *J. Basic Eng.*, **94**, 142–146.

[5] Chikanawa, K., Yoshida, S., Hong, H., & Horio, H., 1996, Generation, growth and collapse of a bubble in conductive liquid heated directly by electric current, *JSME Int. J.*, **B39**, 789–797.

[6] Giavedoni, M.D. & Saita, F.A., 1997, The axisymmetric and plane cases of a gas phase steadily displacing a Newtonian liquid – a simultaneous solution of the governing equations, *Phys. Fluids*, **9**, 2420–2428.

[7] Giavedoni, M.D. & Saita, F.A., 1999, The rear meniscus of a long bubble steadily displacing a Newtonian liquid in a capillary tube, *Phys. Fluids*, **11**, 786–794.

[8] Oğuz, H.N. & Prosperetti, A., 1998, The natural frequency of oscillation of gas bubbles in tubes, *J. Acoust. Soc. Am.*, **103**, 3301–3308.

[9] Oğuz, H.N. & Zeng, J., 1997, Axisymmetric and three–dimensional boundary integral simulations of bubble growth from an underwater orifice, *Engineering Analysis with Boundary Elements*, **19**, 319–330.

[10] Olbricht, W.L., 1996, Pore–scale prototypes of multiphase flow in porous media, *Ann. Rev. Fluid Mech.*, **28**, 187–213.

[11] Peng, X.F., Hu, H.Y., & Wang, B.X., 1998, Boiling nucleation during liquid flow in microchannels, *Int. J. Heat Mass Transfer*, **41**, 101–106.

[12] Peng, X.F. & Wang, B.X., 1994, Liquid flow and heat transfer in microchannels with/without phase change, in *Proceedings of the 10th International Heat Transfer Conference*, Hewitt, G., ed., Ind. Eng. Chem., 159–177.

[13] Plesset, M.S. & Prosperetti, A., 1977 Bubble dynamics and cavitation, *Ann. Rev. Fluid Mech.*, **9**, 145–185.

[14] Popinet, S. & Zaleski, S., 1999, A front–tracking algorithm for accurate representation of surface tension, *Int. J. Numer. Meth. Fluids*, **30**, 775–793.

[15] Satik, C. & Yortsos, 1996, A pore–network study of bubble growth in porous media driven by heat transfer, *J. Heat Transfer*, **118**, 455–462.

[16] Scardovelli, R. & Zaleski S., 1999, Direct numerical simulation of free–surface and interfacial flow, *Ann. Rev. Fluid Mech.*, **31**, 567–603.

[17] Wilson, S. K., Davis, S. H., & Bankoff, S. G., 1999, The unsteady expansion and contraction of a long two–dimensional vapour bubble between superheated or subcooled parallel plates, *J. Fluid Mech.*, **391**, 1–27.

[18] Yuan, H., Oğuz, H.N., & Prosperetti, A., 1999, Growth and collapse of a vapor bubble in a small tube, *Int. J. Heat Mass Transfer*, **42**, 3643–3657.

[19] Yuan, H. & Prosperetti, A., 1999, The pumping effect of growing and collapsing bubbles in a tube, *J. Micromech. Microeng.*, **9**, 402–413.

[20] Zaleski, S., Li, J., Succi, S., Scardovelli, R., & Zanetti, G., 1995, Direct numerical simulation of flows with interfaces, in *Proceedings of the 2nd International Conference on Multiphase Flow*, Serizawa, A., Fukano, T., & Bataille, J., eds., Kyoto, ICMF95, PT2–1 –PT2–12.

TABLES

Figure #	$\mathcal{P}$	Re	We	St	$\mathcal{A}$	$\mathcal{T}_v$	$\mathcal{T}_d$	$\mathcal{T}_\sigma$
2	50	306.25	21.44	12.76	32	0.16	66.14	0.59
3	50	51.04	21.44	12.76	32	0.39	11.02	0.59
6	50	306.25	114.33	12.76	32	0.16	28.64	1.37
7	50	306.25	10.72	12.76	32	0.16	93.54	0.42
8	50	306.25	21.44	76.53	32	0.07	66.14	3.54
9	50	306.25	21.44	2.39	32	0.37	66.14	0.11
11	100	306.25	21.44	12.76	32	0.23	66.14	0.30
12	12.5	306.25	21.44	12.76	32	0.08	66.14	2.36
14	50	306.25	21.44	12.76	8	0.16	66.14	0.59
15	50	306.25	21.44	12.76	64	0.16	66.14	0.59
16 & 17	50	612.5	85.75	3.19	32	0.23	66.14	0.30

TABLE I. Values of various dimensionless parameters used in the figures of this article.

TABLE CAPTION

I. Values of various dimensionless parameters used in the figures of this article.

FIGURE CAPTIONS

1. Sketch of the situation modelled in this paper. The computational domain is limited to the interior of the tube and is bounded by the dashed lines at the tube ends.

2. Bubble shape at different instants during growth (upper panel) and collapse (lower panel); here and in the following the last computed shape in the upper panel is repeated in the lower one. The dimensionless parameters have values $\mathcal{A} = 32$, $Re = 306.25$, $St = 12.76$, $We = 21.44$ (see Table). Because of symmetry, only the right half of the bubble is shown. Note that the actual computational domain extends between $z/D = -16$ and $z/D = 16$ and therefore considerably beyond the left and right frame boundaries. Successive bubble shapes are separated by 3.92×10^{-3} dimensionless time units.

3. As in Fig. 2 except that $Re = 51.04$. Successive bubble shapes are separated approximately by 4.54×10^{-3} dimensionless time units.

4. Bubble volume vs. time for different values of the Reynolds number; all other parameter values as in Fig. 2. The dashed line differs from the adjacent solid line only in that the condition $P_e = P_\infty$ is applied during both the growth and collapse phases.

5. Bubble lifetime (circles, left scale) and maximum bubble volume (squares, right scale) vs. Reynolds number; all other parameter values as in Fig. 2.

6. As in Fig. 2 except that $We = 114.33$. Successive bubble shapes are separated approximately by 4.04×10^{-3} dimensionless time units.

7. As in Fig. 2 except that $We = 10.72$. Successive bubble shapes are separated approximately by 2.67×10^{-3} dimensionless time units.

8. As in Fig. 2 except that $St = 76.53$. Successive bubble shapes are separated approximately by 1.29×10^{-2} dimensionless time units.

9. As in Fig. 2 except that $St = 2.39$. Successive bubble shapes are separated approximately by 1.22×10^{-3} dimensionless time units.

10. Bubble volume vs. time for different values of the Strouhal number; all other parameter values as in Fig. 2.

11. As in Fig. 2 except that $\mathcal{P} = 100$. Successive bubble shapes are separated approximately by 3.7×10^{-3} dimensionless time units.

12. As in Fig. 2 except that $\mathcal{P} = 12.5$. Successive bubble shapes are separated approximately by 2.46×10^{-3} dimensionless time units.

13. Bubble volume vs. time for different values of the pressure ratio; all other parameter values as in Fig. 2.

14. As in Fig. 2 except that $\mathcal{A} = 8$. The computational domain extends between $z/D = -4$ and $z/D = 4$. Successive bubble shapes are separated approximately by 3×10^{-3} dimensionless time units.

15. As in Fig. 2 except that $\mathcal{A} = 64$. The computational domain extends between $z/D = -32$ and $z/D = 32$. Successive bubble shapes are separated approximately by 3.1×10^{-3} dimensionless time units.

16. Successive shapes during growth (upper panel) and collapse (lower panel) of a bubble initiated at a distance equal to 3/8 of the tube length from the left–end of the tube. The dimensional parameters have the same value as in Fig. 2 except that $\tau = 2$ μs. Note that the

computational domain extends between $z = 0$ and $z = 2000$ μm and therefore considerably beyond the left and right frame boundaries. The separation between consecutive bubble shapes is approximately 2.6 μs.

17. Liquid velocity induced by the bubble growth and collapse on the axis of symmetry at the left (solid line) and right (dashed line) ends of the tube for the case of the previous figure. Note that at the end of the collapse there is a residual velocity away from the left end of the tube.

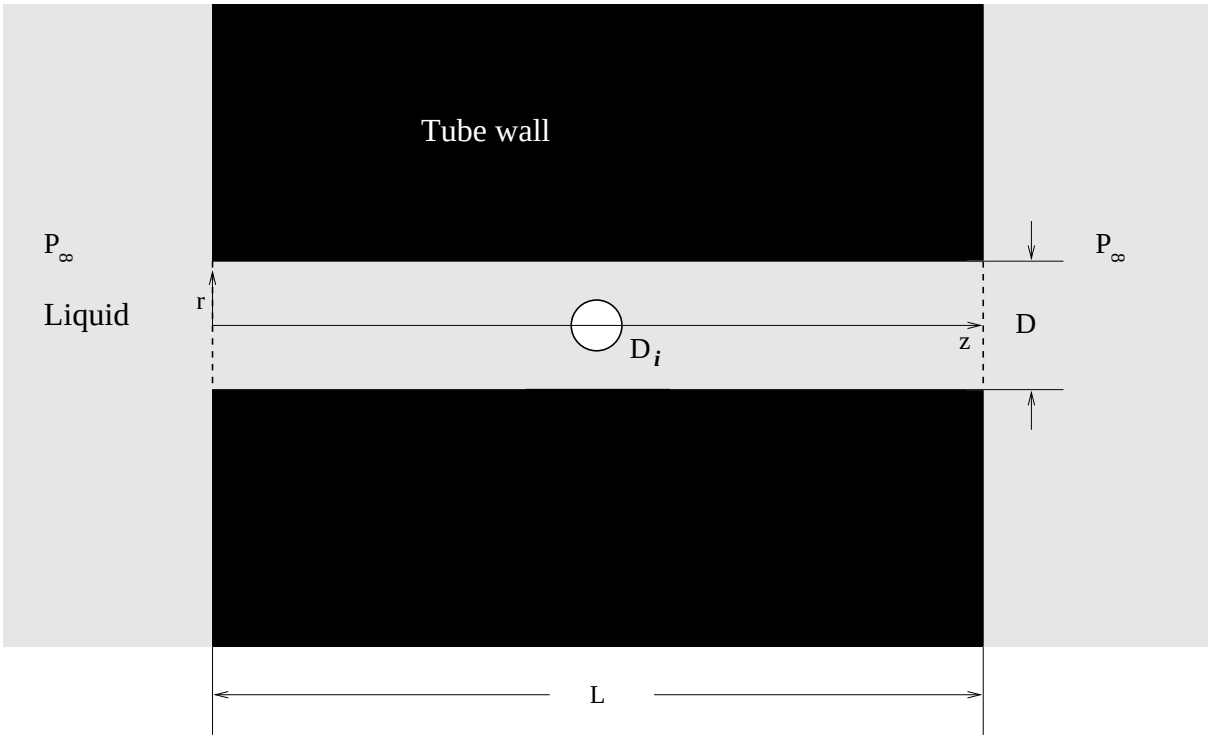

FIG. 1.

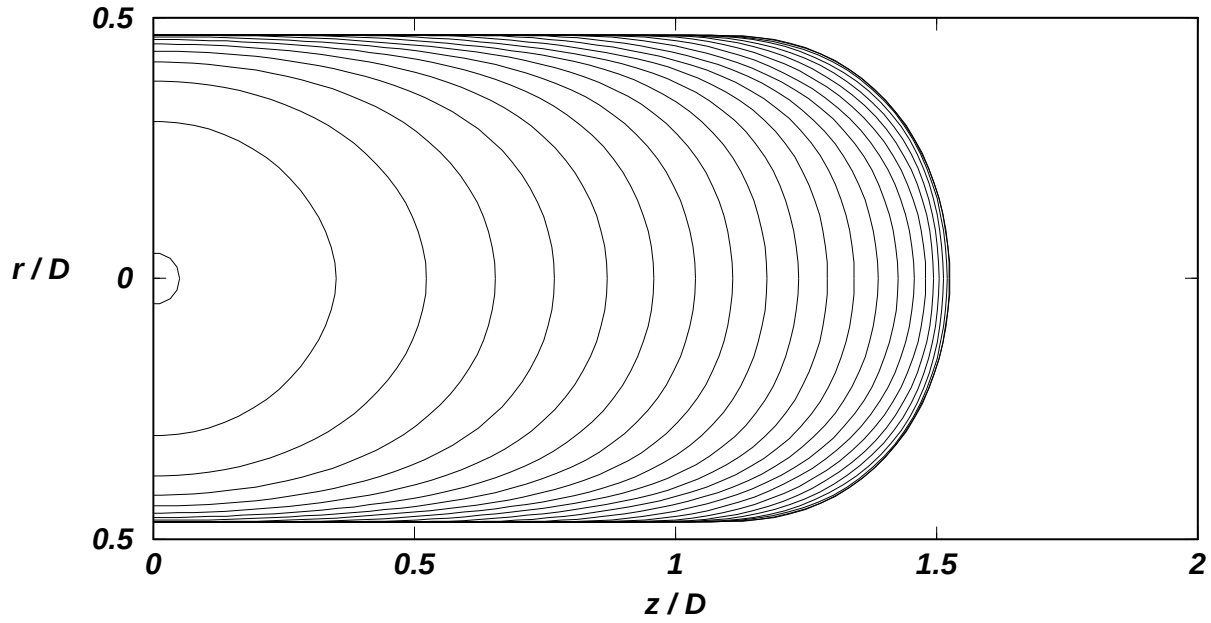

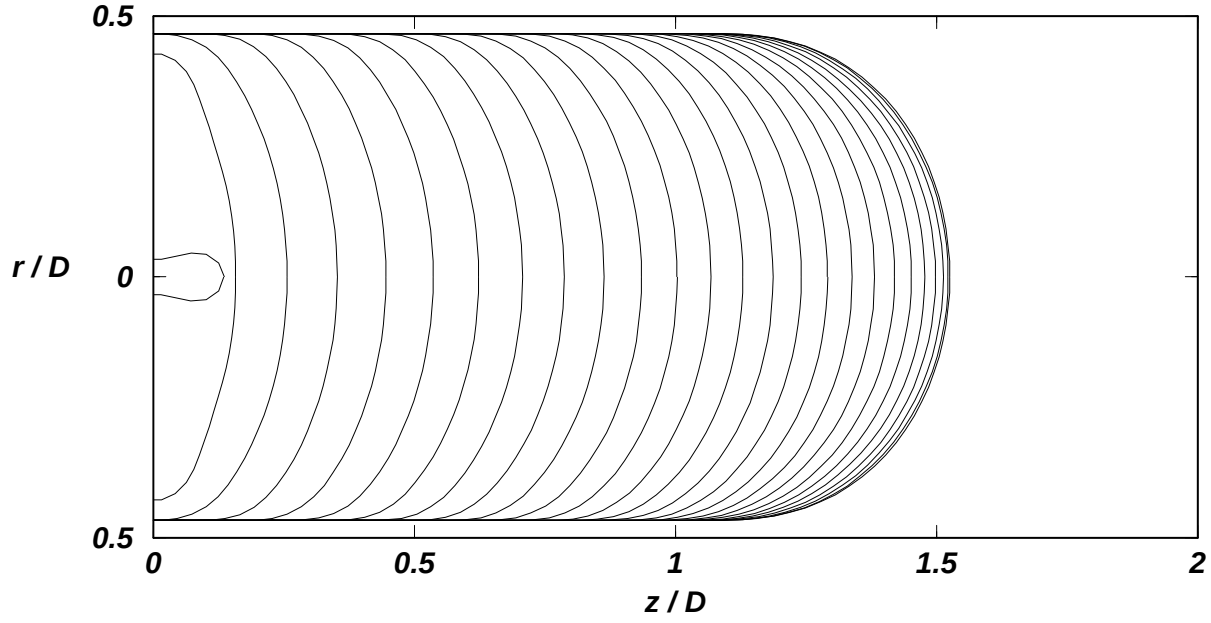

FIG. 2.

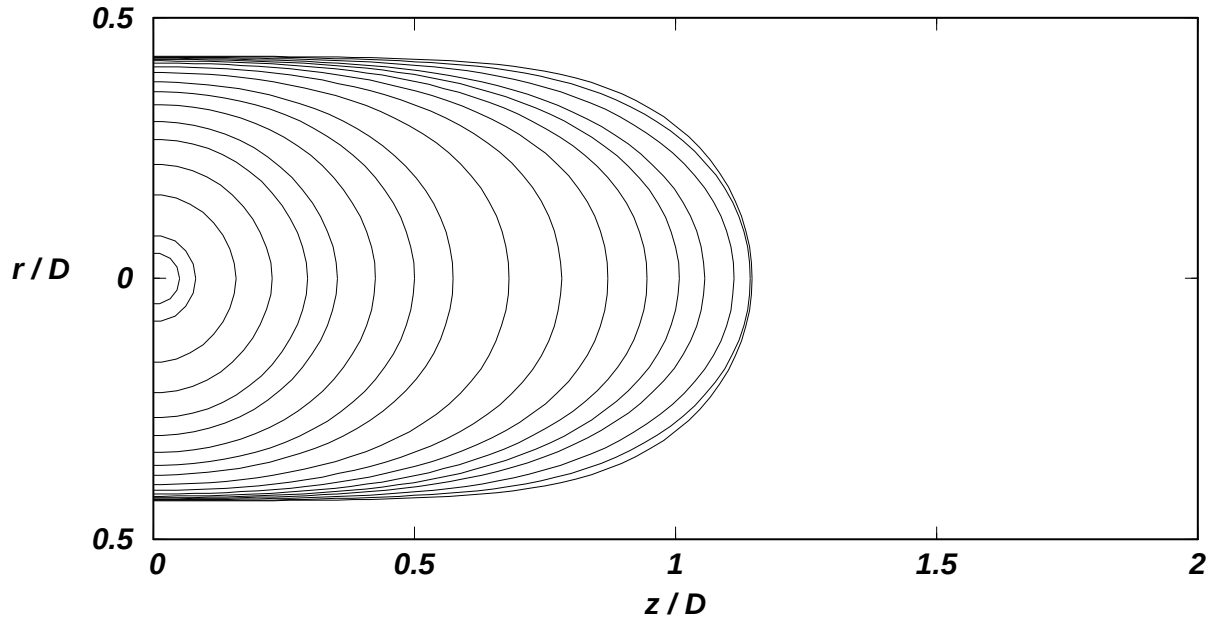

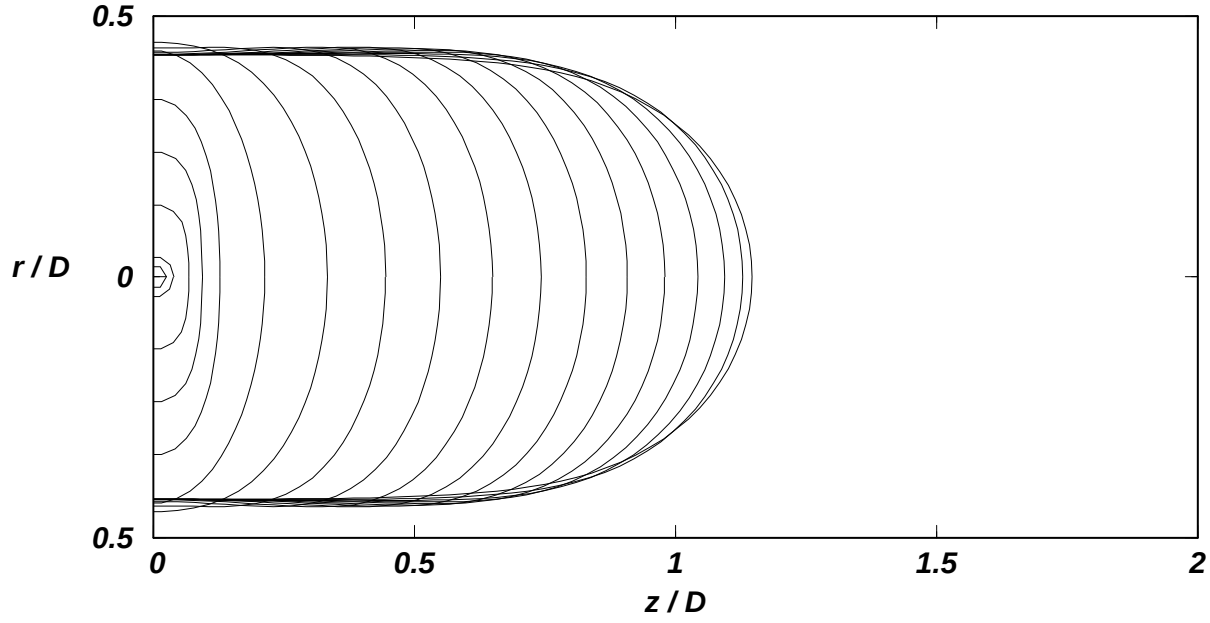

FIG. 3.

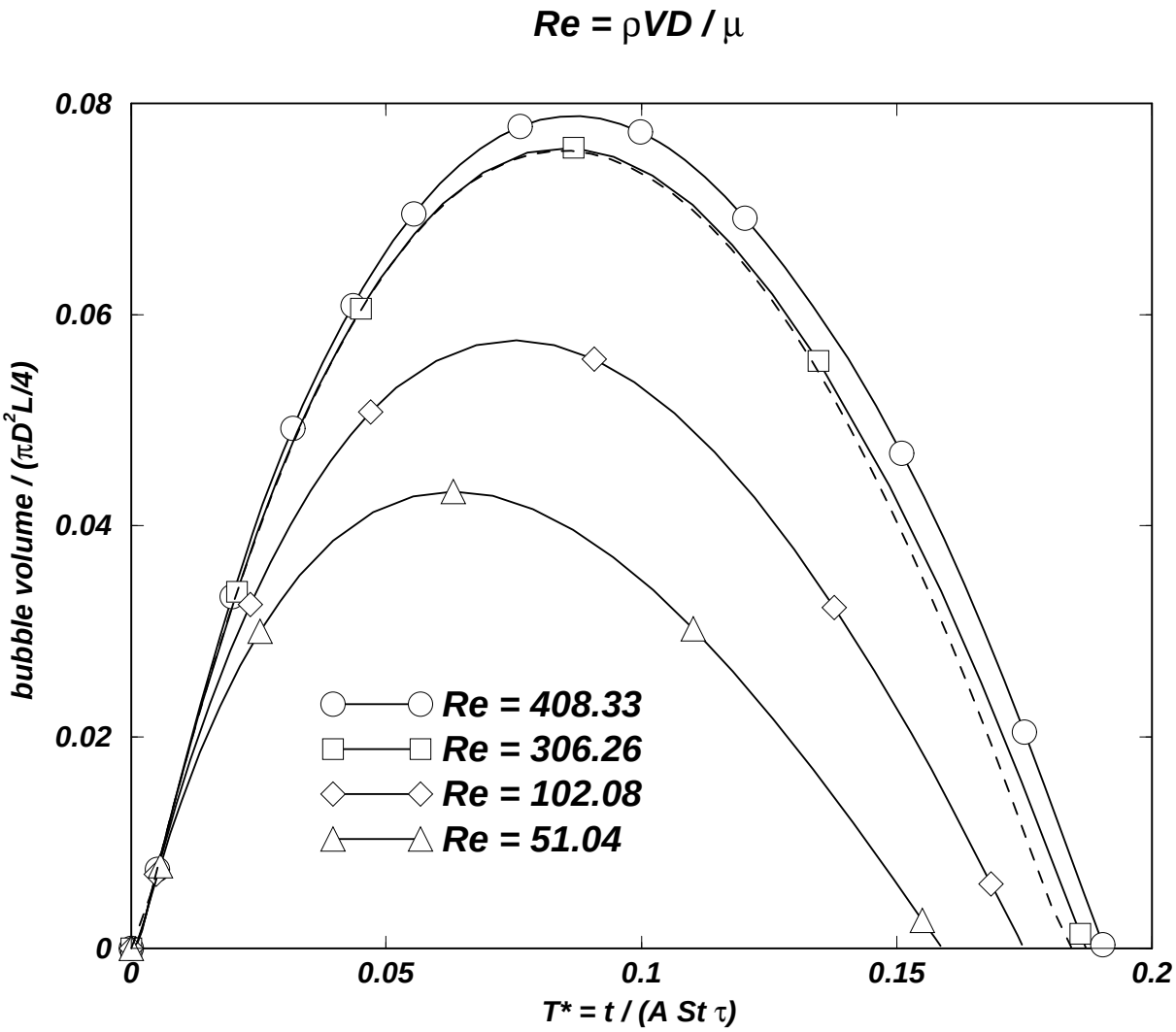
Re = ρVD / μ
0.08
0.06
0.04
0.02
0
bubble volume / (πD²L/4)
0
0.05
0.1
0.15
0.2
T* = t / (A St τ)
Re = 408.33
Re = 306.26
Re = 102.08
Re = 51.04

FIG. 4.

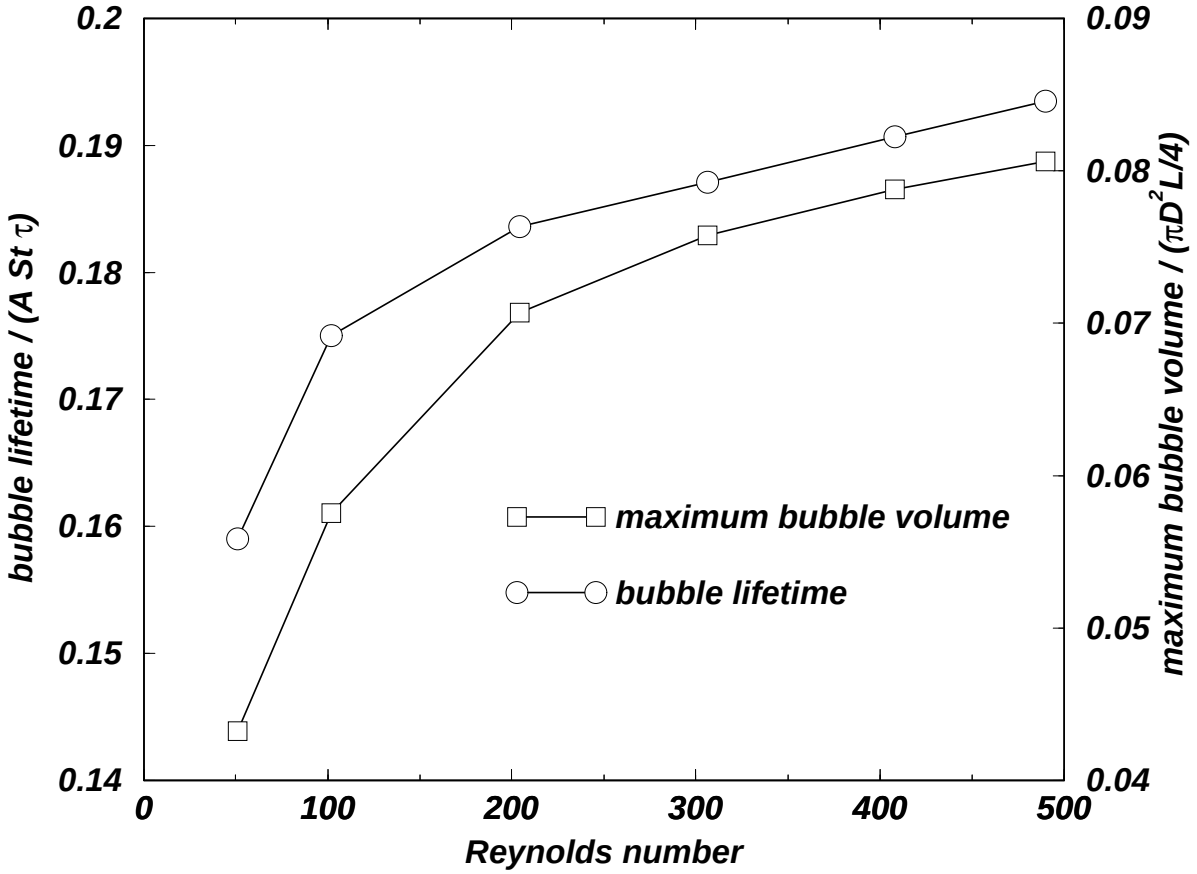
0.2
0.19
0.18
0.17
0.16
0.15
0.14
0.09
0.08
0.07
0.06
0.05
0.04
0
100
200
300
400
500
Reynolds number
bubble lifetime / (A St τ)
maximum bubble volume / (πD²L/4)
maximum bubble volume
bubble lifetime

FIG. 5.

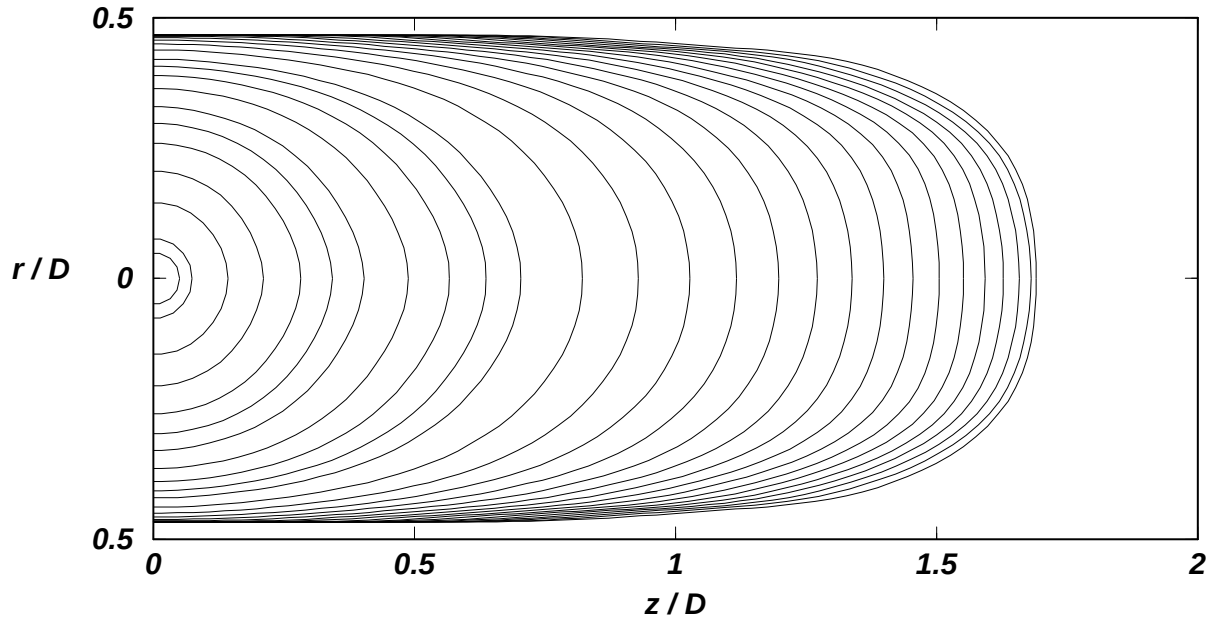

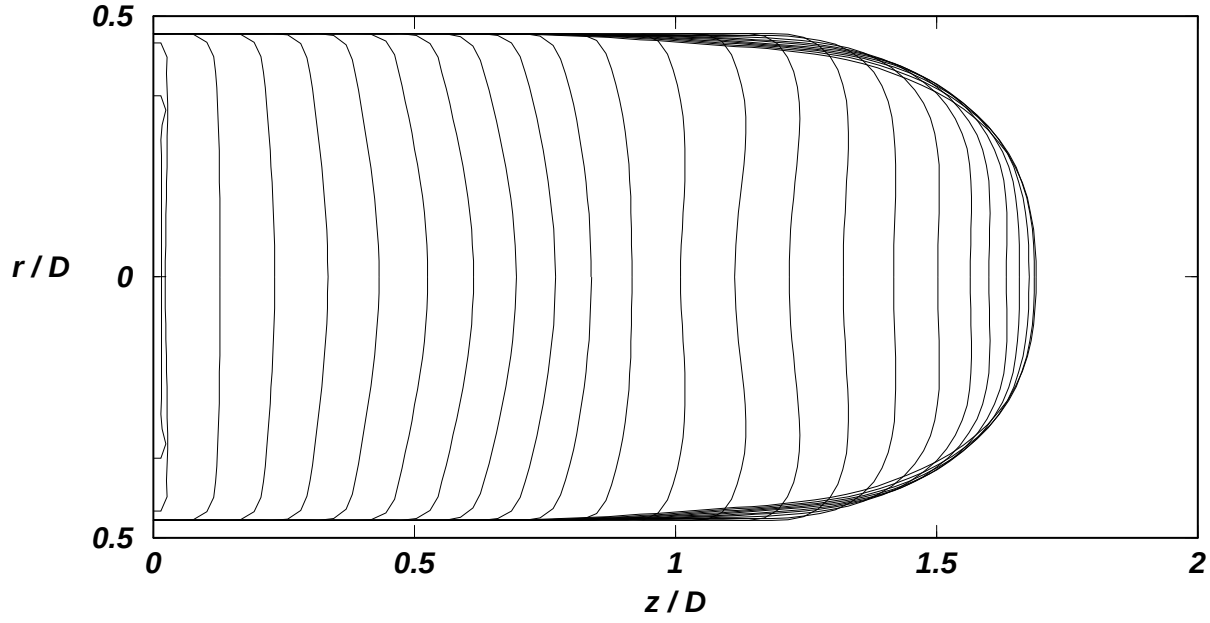

FIG. 6.

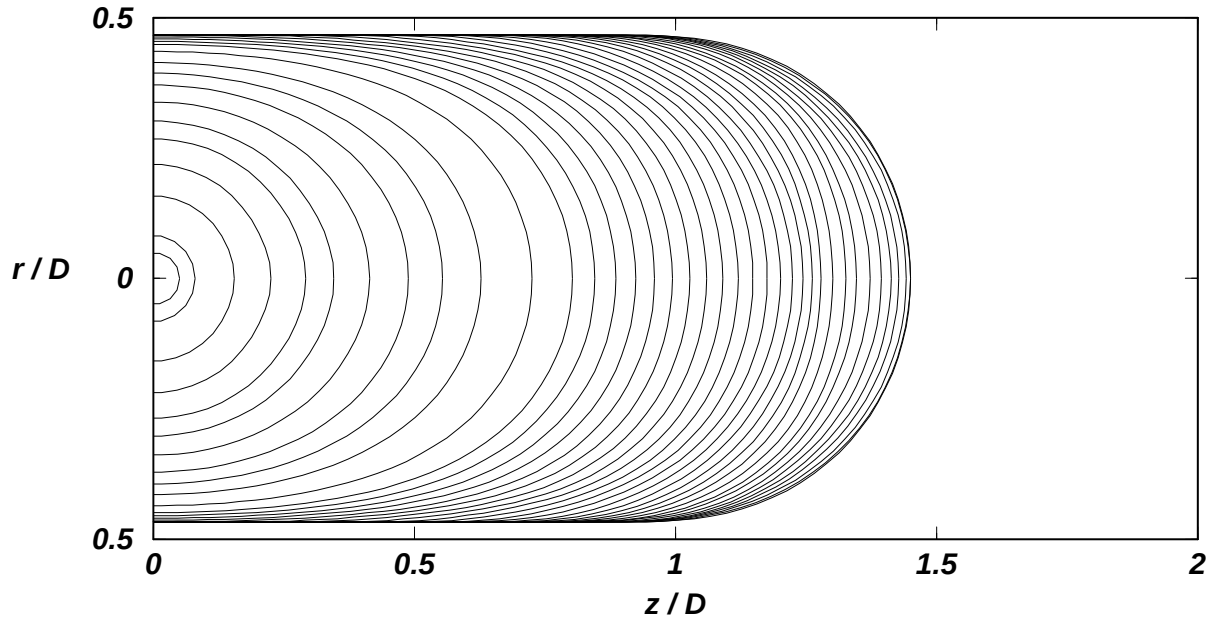

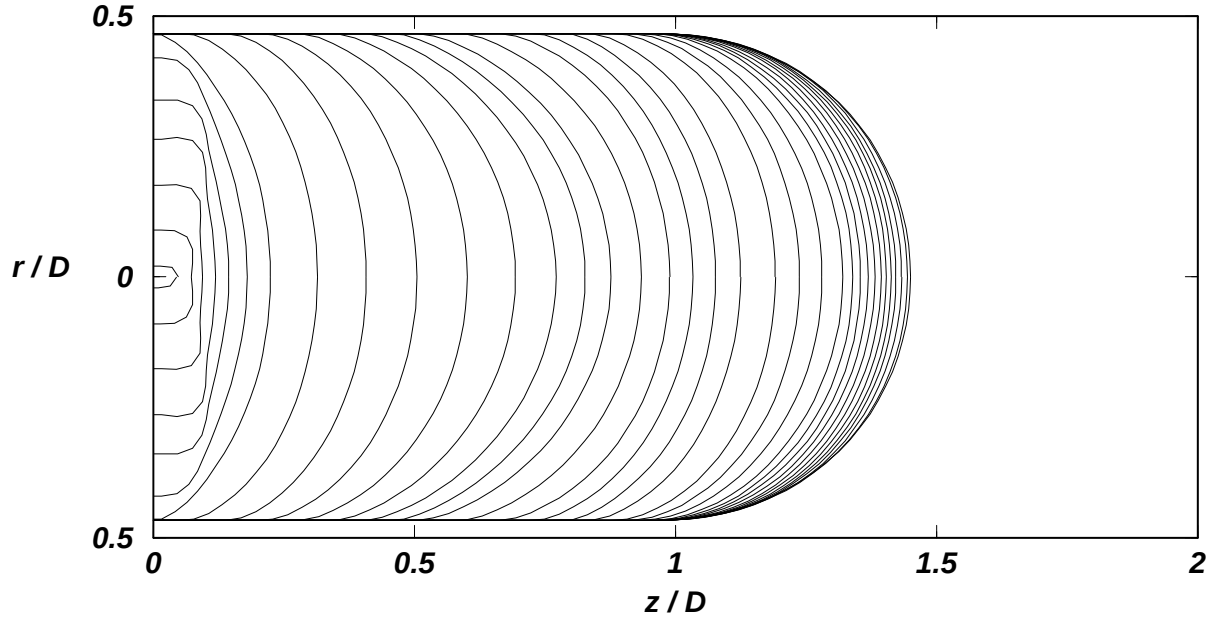

FIG. 7.

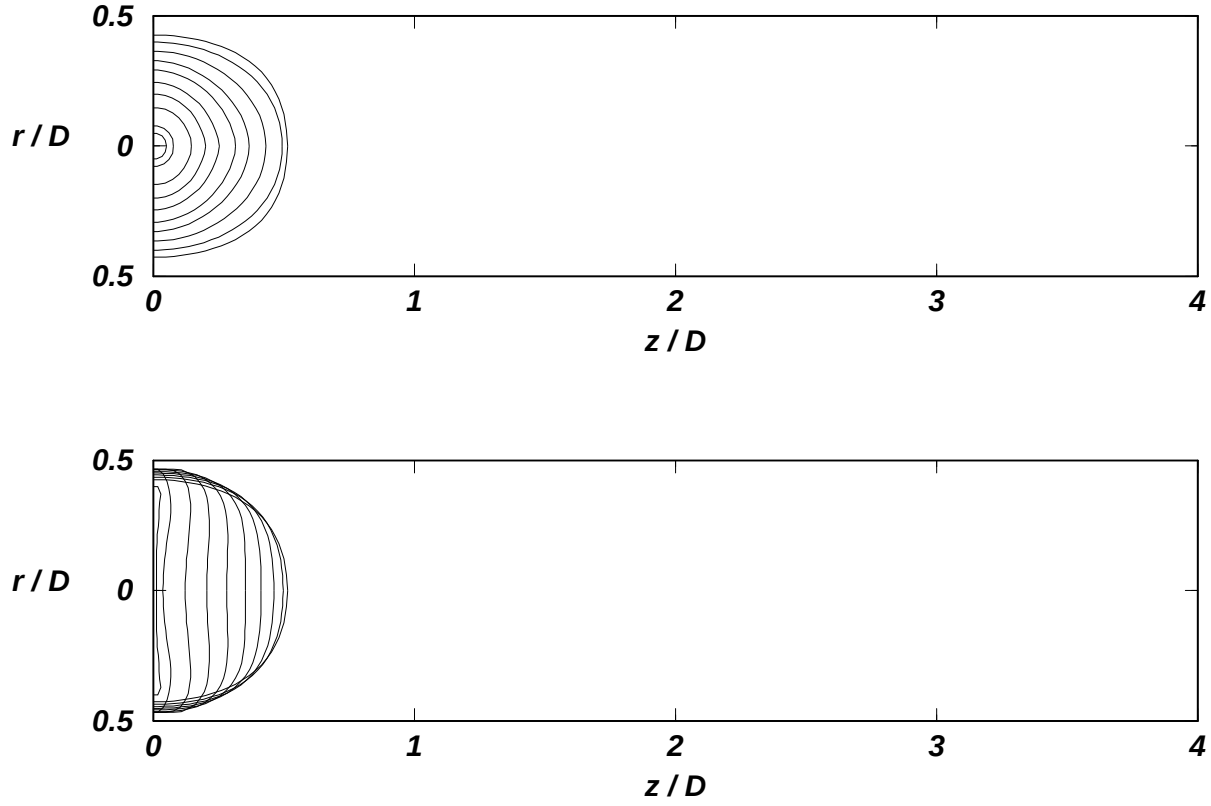

FIG. 8.

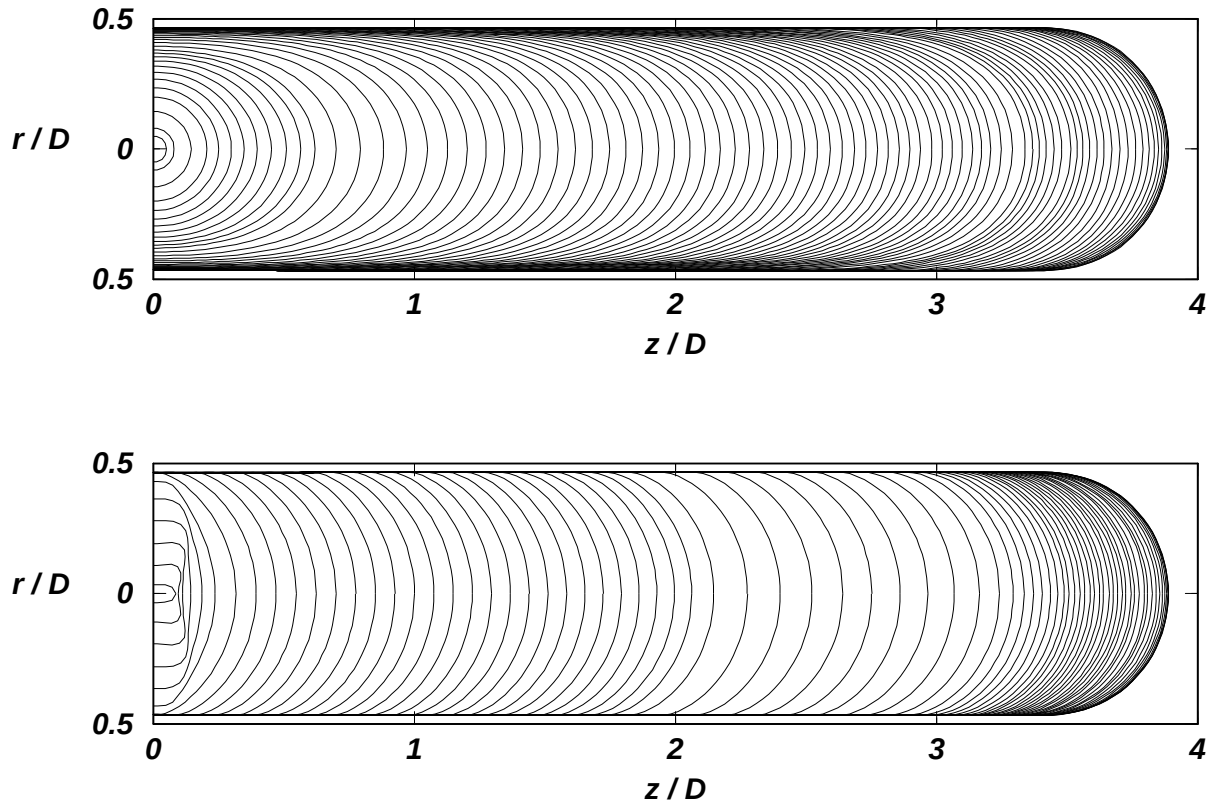

FIG. 9.

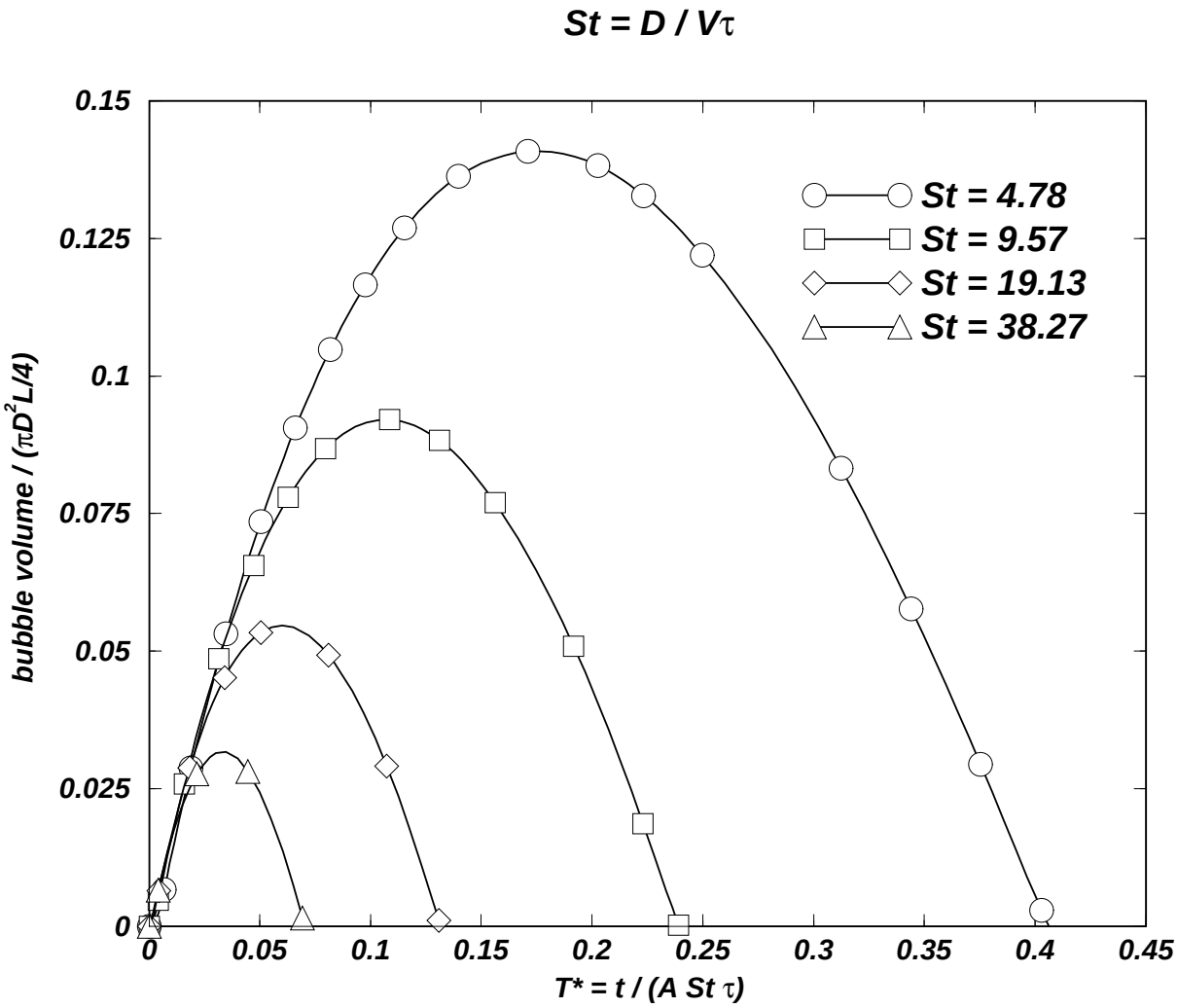
St = D / Vτ
0.15
0.125
0.1
0.075
0.05
0.025
0
bubble volume / (πD²L/4)
0
0.05
0.1
0.15
0.2
0.25
0.3
0.35
0.4
0.45
T* = t / (A St τ)
St = 4.78
St = 9.57
St = 19.13
St = 38.27

FIG. 10.

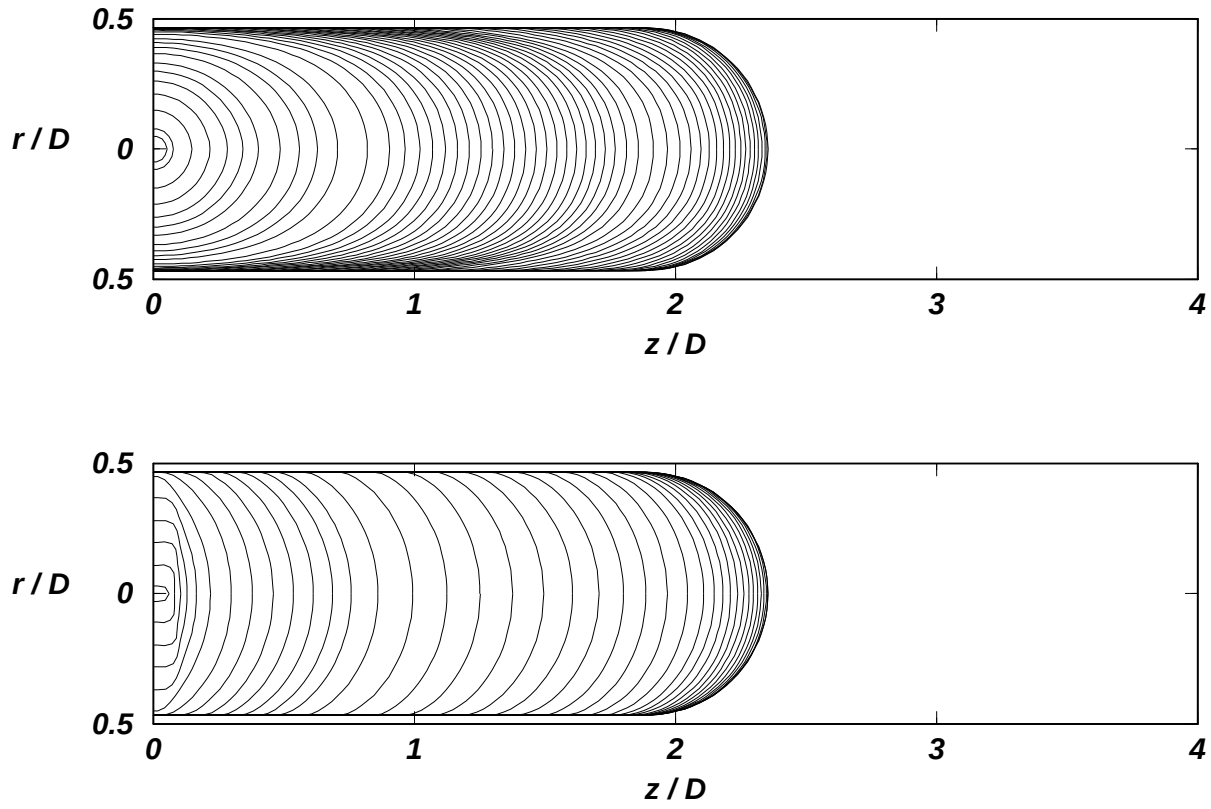

FIG. 11.

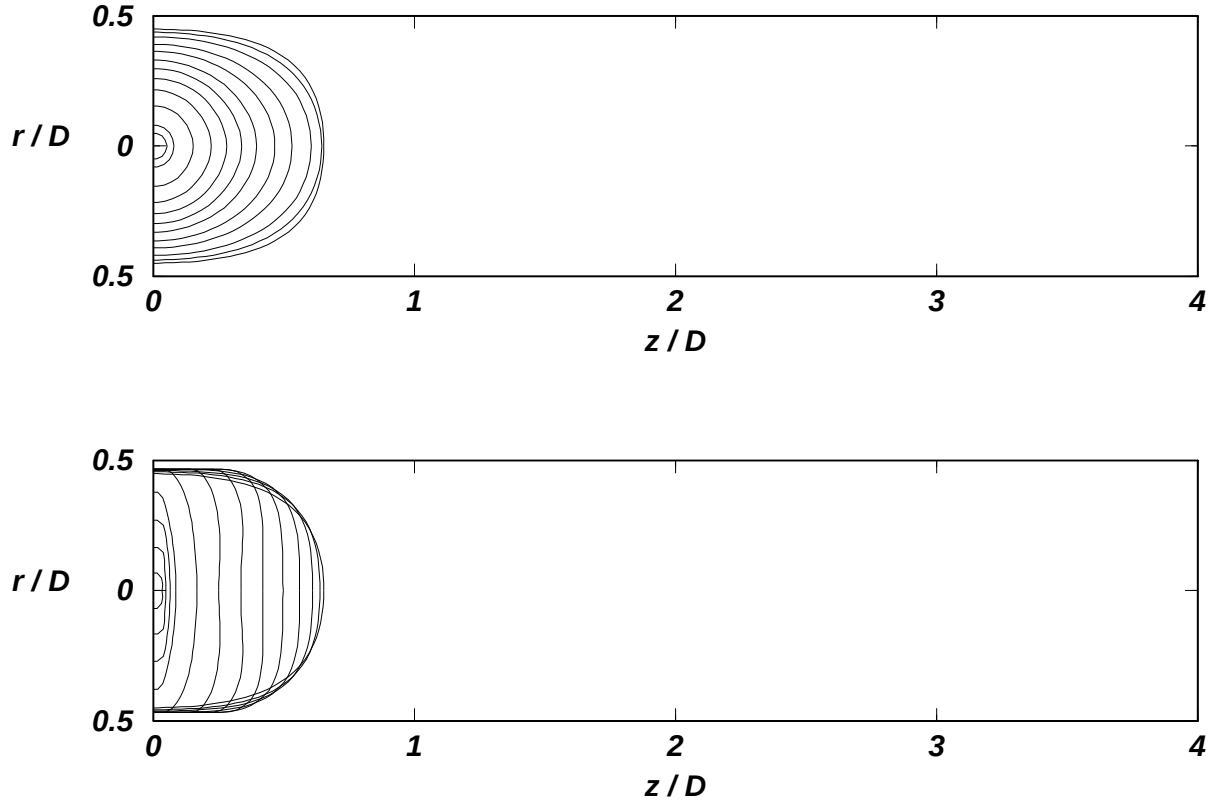

FIG. 12.

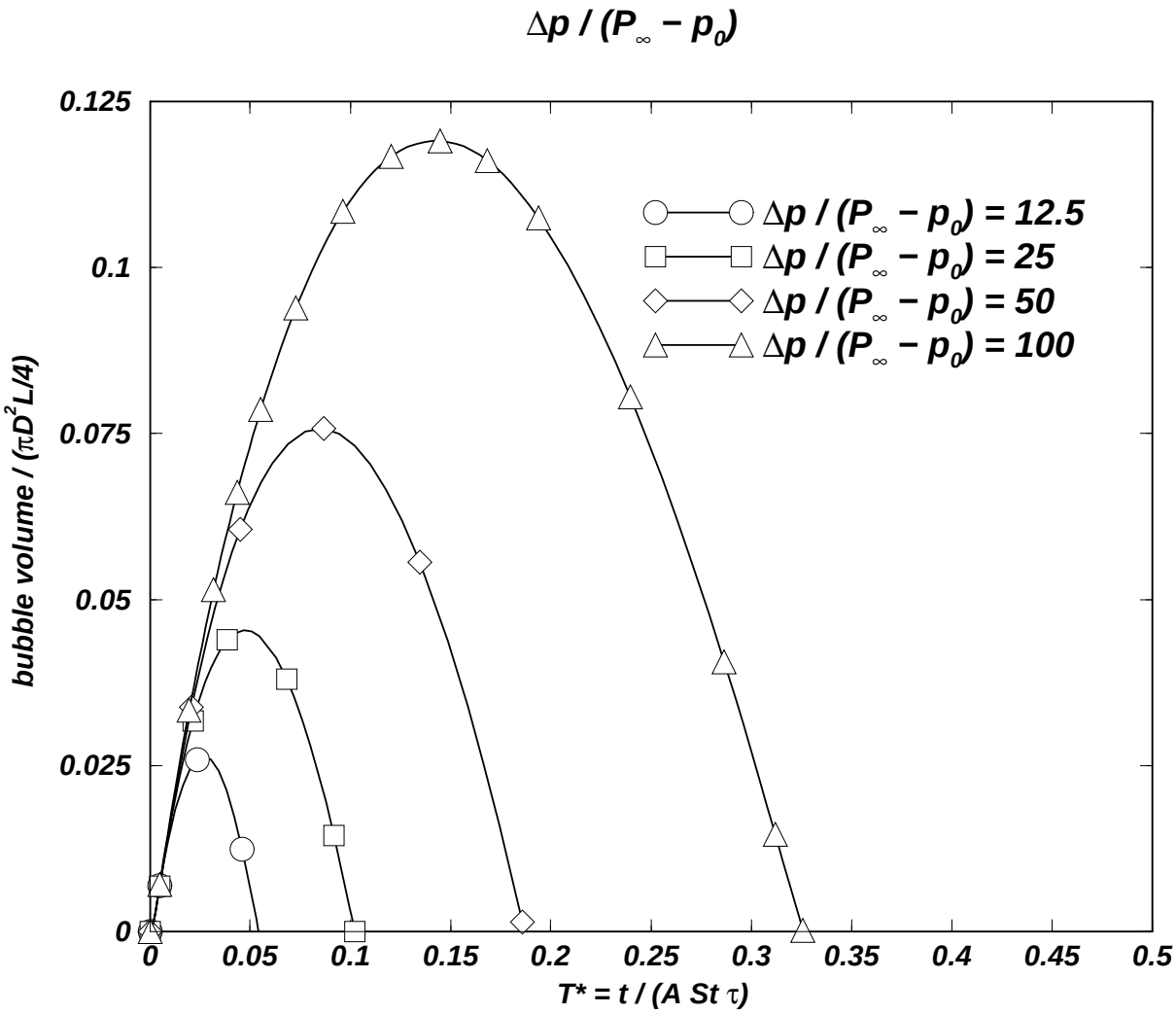
Δp / (P∞ − p0)
0.125
0.1
0.075
0.05
0.025
0
bubble volume / (πD²L/4)
0
0.05
0.1
0.15
0.2
0.25
0.3
0.35
0.4
0.45
0.5
T* = t / (A St τ)
Δp / (P∞ − p0) = 12.5
Δp / (P∞ − p0) = 25
Δp / (P∞ − p0) = 50
Δp / (P∞ − p0) = 100

FIG. 13.

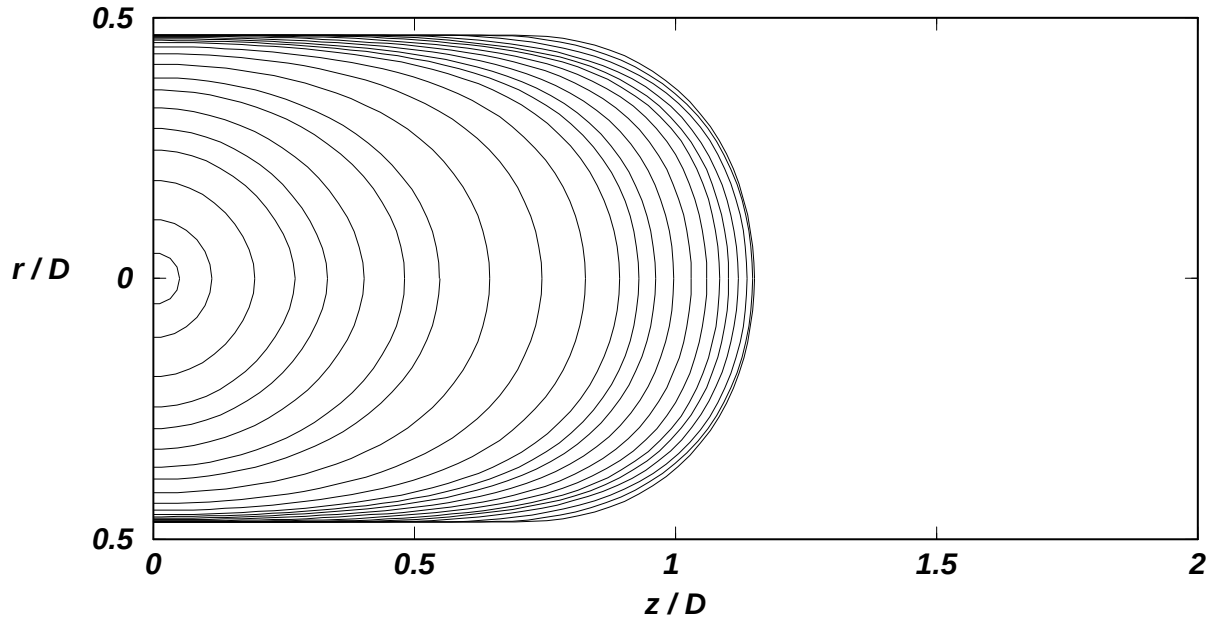

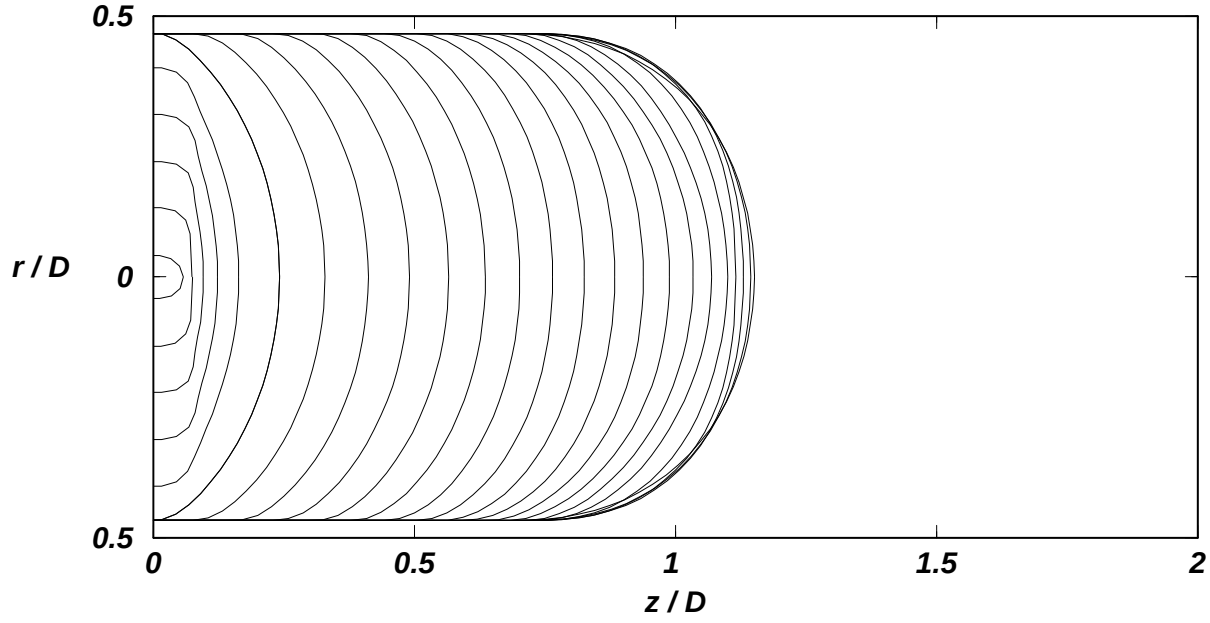

FIG. 14.

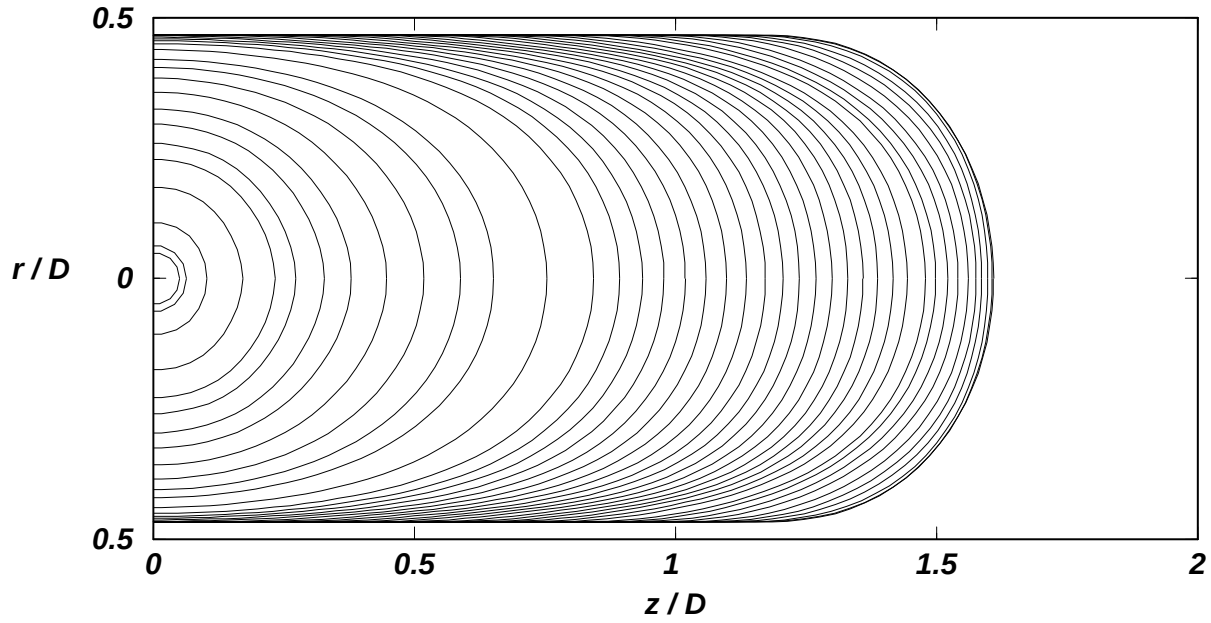

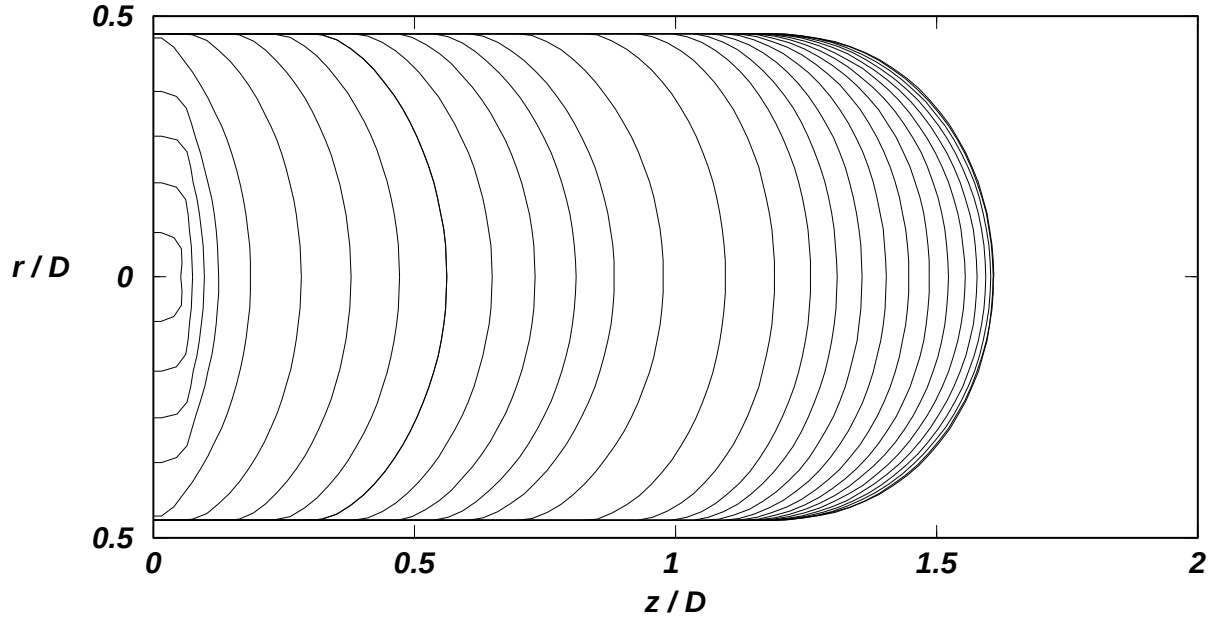

FIG. 15.

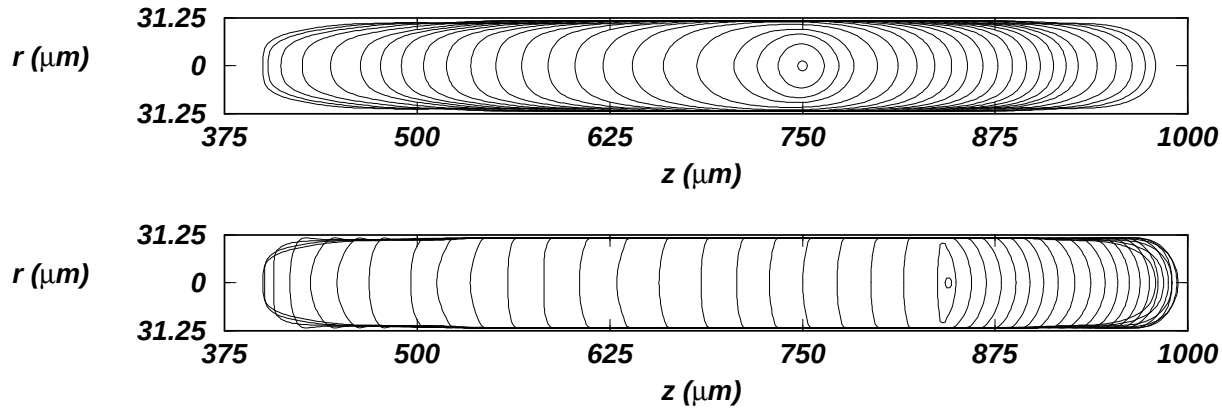
r (μm)
31.25
0
31.25
375
500
625
750
875
1000
z (μm)
r (μm)
31.25
0
31.25
375
500
625
750
875
1000
z (μm)

FIG. 16.

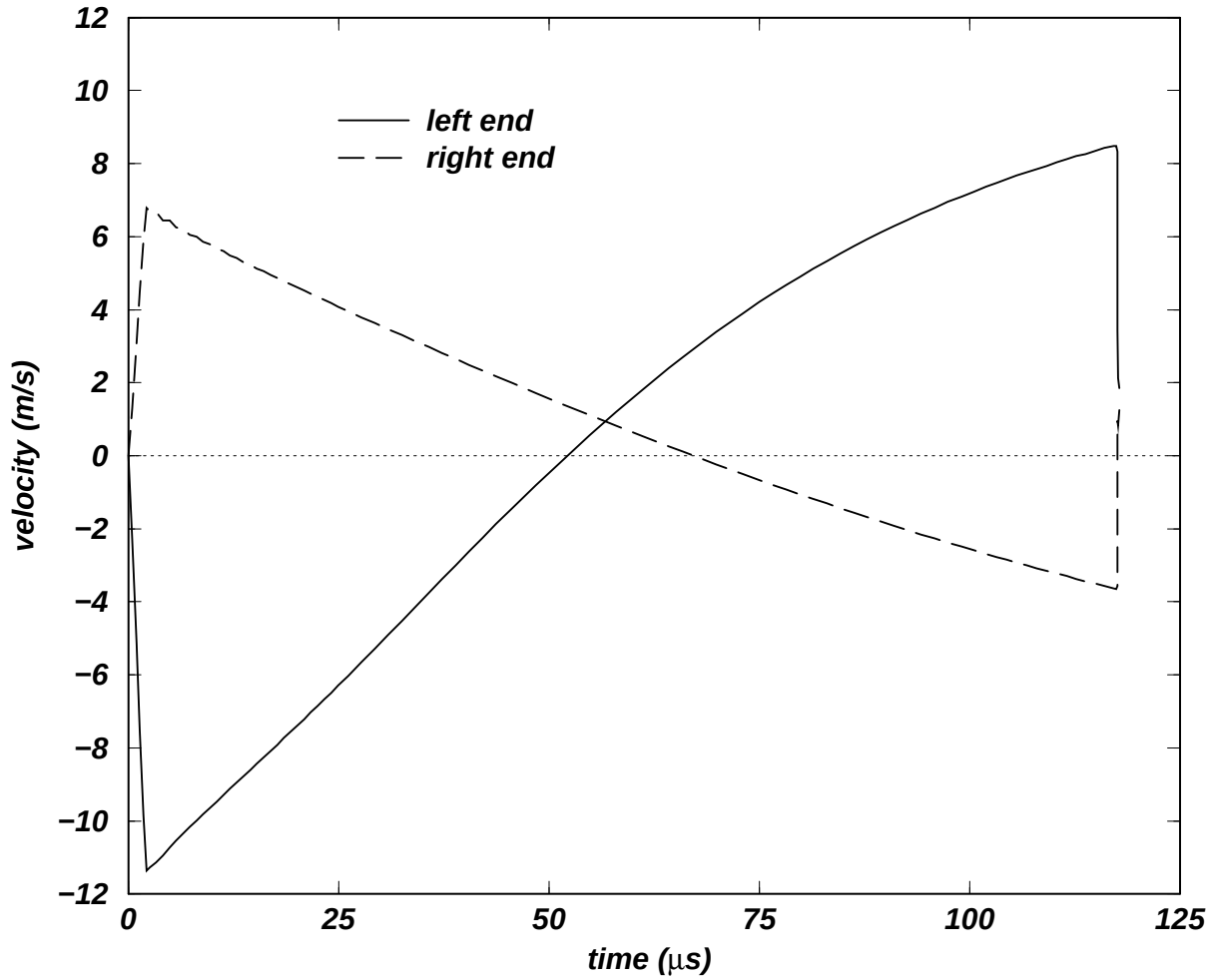
12
10
8
6
4
2
0
−2
−4
−6
−8
−10
−12
0
25
50
75
100
125
velocity (m/s)
time (μs)
left end
right end

FIG. 17.